CSIRO PUBLISHING

International Journal of Wildland Fire **2018**, *27*, 800–814
https://doi.org/10.1071/WF17126

Simulation study of grass fire using a physics-based model: striving towards numerical rigour and the effect of grass height on the rate of spread

K. A. M. Moinuddin[A,B,E], *D. Sutherland*[A,B,*] and *W. Mell*[D]

[A]Centre for Environmental Safety and Risk Engineering, Victoria University, Melbourne 8001, Vic., Australia.
[B]Bushfire and Natural Hazards Cooperative Research Centre, 340 Albert Street, East Melbourne, Vic., Australia.
[C]Department of Mechanical Engineering, University of Melbourne, Parkville 3010, Vic., Australia.
[D]US Forest Service, Pacific Wildland Fire Sciences Laboratory, Seattle, WA 98103, USA.
[E]Corresponding author. Email: khalid.moinuddin@vu.edu.au

Abstract. Grid-independent rate of spread results from a physics-based simulation are presented. Previously, such a numerical benchmark has been elusive owing to computational restrictions. The grid-converged results are used to systematically construct correlations between the rate of spread (RoS) and both wind speed and grass height, separately. The RoS obtained from the physics-based model is found to be linear with wind speed in the parameter range considered. When wind speed is varied, the physics-based model predicts faster RoS than the Mk III and V (McArthur) models (Noble *et al.* 1980) but slower than the CSIRO model (Cheney *et al.* 1998). When the grass height is varied keeping the bulk density constant, the fire front changes from a boundary layer flame mode to plume flame mode as the grass height increases. Once the fires are in plume mode, a higher grass height results in a larger heat release rate of the fire but a slower RoS.

Additional keywords: atmospheric boundary layer, operational model, physics-based modelling, wildland fire, wind speed.

Received 21 August 2017, accepted 25 September 2018, published online 2 November 2018

Introduction

Wildland fires or bushfires, as they are called in Australia, are the uncontrolled spread of fires that occur in areas of countryside or wilderness. In recent events, bushfires have encroached on the built environment, causing injuries, fatalities and loss of property. The magnitude and severity of a bushfire are results of complex physical and chemical processes that operate on vastly different scales, affected by topography, varying climate conditions and the type of the vegetative or solid fuels.

In extreme drought and heat wave conditions, with temperatures in excess of 40°C and high wind speeds with gusts in excess of 100 km h^{-1} (Bureau of Meteorology 2009), a fire catastrophe with dramatically increased fire risks to communities may occur. Ignition could be caused by natural causes such as lightning, embers from other fires or human causes, either accidental or deliberate.

The spread of the fire depends particularly on the wind speed and to a slightly lesser extent, the rate of spread (RoS) depends on various factors including the type of fuel, height, density and moisture content of the fuel and ambient conditions (McArthur 1967). Until fires reach the wildland–urban interface, the fuels are mainly vegetative, such as litter, trees, shrubs and grass.

Bushfires in many countries pose a serious threat to the homes of people that reside in close proximity to rural, grassland and forested areas. The fires caused in these areas can also impact on the viability of the surrounding region. This includes disruption in water supplies due to erosion and contamination caused by the fires. The incidence of fires attracts much public concern owing to their devastating effects, as exemplified in the cases of Black Saturday of 2009 and Ash Wednesday of 1983 in Australia and the 2009 bushfires in Athens and Los Angeles. Therefore, it is important to conduct studies on the behaviour of fire spread, although this is typically difficult because the sizes and RoS depend on various topographical (aspect and slope), fuel (density, height, homogeneity and moisture) and weather (wind, temperature and humidity of the air, soil moisture, etc.) parameters.

*D. Sutherland is now affiliated with School of Physical Environmental and Mathematical Sciences (PEMS), University of New South Wales, Canberra. 2610, ACT, Australia

Experimental studies are limited by the ability of researchers to safely conduct controlled experiments. Hence, experimental fires tend to represent the fire in benign weather conditions (such as under 30°C and wind speed less than 10 m s^{-1}) and not representative of conditions leading to dangerous and destructive bushfires.

Recently, there has been increased interest in physics-based fire simulation. This approach uses the fundamental equations governing fluid transport, heat transfer, combustion and thermal decomposition of materials to simulate a fire. Several physics-based studies have been conducted to model two-dimensional (2-D) fire spread in pine needles (Morvan and Dupuy 2001) and Mediterranean shrubland fuels (Morvan and Dupuy 2004) and grassland (Morvan *et al.* 2009). These studies focused on simulating vertical planar slices of fire spread. That is, the flame is simulated in the direction of fire spread and the vertical direction. It is important to distinguish these 2-D simulations from simulations of fire spread where the fire front is represented as a 2-D contour in the *xy* plane. In simulators such as Spark (Miller *et al.* 2015) or Phoenix RapidFire (Chong *et al.* 2012), the fire front evolves in two spatial dimensions, using some empirical or kinematic model for spread rate where the physics of the combustion and flame are neglected. Although the full physics-based 3-D simulation approach is limited largely by computational resources, it is more closely related to real-life physical phenomena. The 2-D approach of Morvan and Dupuy (2001, 2004), Morvan *et al.* (2009) neglects fundamental mechanisms of fluid turbulence production, and neglects the effects associated with the fire front curvature (Linn *et al.* 2012). Three-dimensional physics-based models can be used to extract insight into the detailed behaviour of bushfire spread and bushfire situations that may not be easily obtained from the experimental work.

We are developing and utilising a 3-D physics-based fire model to improve our understanding of how fires propagate through wildland fuels under a variety of weather, fuel configuration and terrain conditions, and how these fires can subsequently ignite structures. The model used in this study is basically an extension of National Institute of Standard and Technology (NIST)'s building fire model Fire Dynamics Simulator (FDS) (McGrattan *et al.* 2013), which is being developed for structural fires. The wildland fire version is named Wildland–Urban Interface Fire Dynamics Simulator (WFDS). Mell *et al.* (2007) used a WFDS version compatible with an earlier version of FDS (version 4) to simulate the same reference grassfire experiment (Cheney *et al.* 1993) modelled in the current study along with another reference case. In both cases, the location of the headfire was well predicted and various grassfire characteristics were reported. The RoS of headfire from WFDS4 were compared with two empirical relations of Cheney *et al.* (1998) as a function of open space velocity 2 m above the ground (U_2) and headfire width developed from experimental data. WFDS4 predictions of RoS dependence on both U_2 wind speed and on the headfire width were similar to an empirical relation. Morvan *et al.* (2013) also used WFDS4 to study the interaction of a forward-propagating (in the direction of the prevailing wind) headfire with a backing fire travelling in the direction opposite to the wind.

In the present study, at first, we strived for a systematic modelling approach to grass fire modelling with WFDS compatible with FDS version 6 (FDSv6). FDSv6 has improved pyrolysis, combustion, radiation and near-wall flow modelling submodels. Its coupled pyrolysis–combustion model (1-D solid and 3-D gas phase) has recently been systematically validated against experimental results (AbuBakar 2016). Importantly, we seek results that are independent of the grid resolution.

The previous studies with FDS and WFDS, in particular Mell *et al.* (2007), had some computational restrictions. In that study, Mell *et al.* reported differences of the order of 10% in the RoS at different resolutions. Computational power has now advanced such that we can use a sufficiently high resolution to ensure grid-independent RoS results.

Once the simulation results are established with some confidence, we investigate the dependence of the RoS on the open wind velocity 10 m above the ground (U_{10}) and grass heights are varied. U_{10} is a standard observation provided by weather stations in Australia and is currently used in operational models. In the operational bushfire forecasting community, the effect of grass height on the RoS is unknown. Recent experiments conducted in Victoria, Australia, (Cruz *et al.* 2016) suggest that RoS does not depend on the grass height. However, observations from gamba grass fires in the Northern Territory, Australia, and other field observations reported by fire agencies suggest that there may be some dependence of RoS on grass height (S. Heemstra, pers. comm. 2016).

Indeed, it would appear intuitive that grass height would be significant in RoS. For example, the taller the grass is, the more drag the grass can exert on the prevailing wind, and the change in wind speed and wind profile will change the RoS of the fire. In the present study, we assume that the grassland bulk density is constant as the height changes.

It is worth noting that the simulations conducted here are designed to replicate the conditions of experimental grass fires. Typically, experimental fires are conducted in fairly benign wind and temperature conditions so that the fires can be easily controlled without posing additional risks.

In summary, we seek to answer the following questions:

- What are the resolution, domain requirements and atmospheric boundary layer establishment time needed to ensure a numerically valid simulation?
- What effect does the grass height have on the RoS of the fire?
- What are the underlying physical mechanisms that govern the RoS changes as the grass fire size increases?

The paper is laid out as follows. First, the physics-based model is briefly reviewed to highlight the differences between the version employed by Mell *et al.* (2007) and the version used here. The development of the atmospheric surface layer above the fire ground is examined and a grid independence study is conducted comparing uniform and stretched grids of different resolutions. Following Mell et al. (2007), the simulation results are compared with the experimental observations of Cheney *et al.* (1993), and the simulation results are found to be valid as expected. Finally, a simulation study where the grass height varies over a range of realistic heights is conducted.

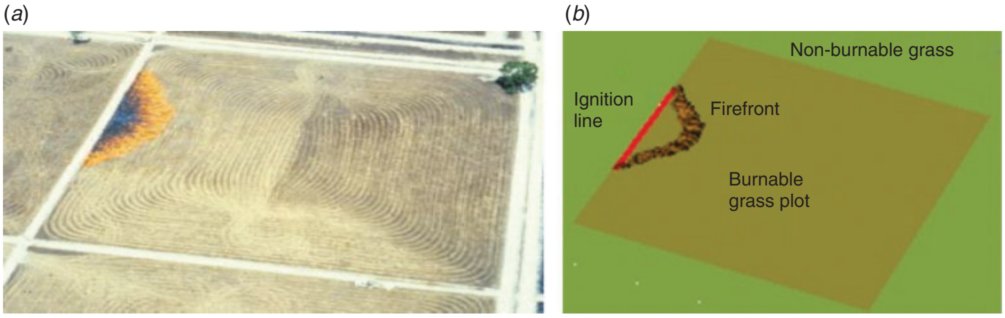

Fig. 1. (*a*) Burning of Australian grassland (Cheney *et al.* 1993); and (*b*) physics-based simulation.

Overview of physics-based model

The WFDS model solves the governing equations for buoyant flow, heat transfer, combustion and thermal degradation of vegetative fuels, and Large Eddy Simulation (LES) techniques are used to solve the gas-phase equations (McGrattan *et al.* 2013). The details of mass and momentum equations including the LES technique and mixture-controlled combustion model can be found in McDermott (2014) and McGrattan *et al.* (2015). The WFDS aims to include fire spread through vegetative fuels. Vegetative fuels can include those characteristic of bushlands, i.e. trees, grasses, understorey growth and ground litter as well as those purchased at nurseries for home or community landscaping purposes such as trees, mulch, grasses and decorative plants. However, in the case of the grasslands considered here, we consider a single uniform vegetation fuel representing grass.

Reference case

Numerical simulations of Australian grassland fires were conducted by CSIRO researchers in Australia (Cheney *et al.* 1993) owing to the simplicity afforded by terrain and (homogeneous) fuel. From that investigation, experimental data were available for two experimental burns for validation of numerical simulations. Predictions of the headfire RoS were considered the key quantity that was studied in relation to these experiments.

One of the abovementioned grassland experiments was conducted on a 104 $\times$ 108-m plot; 4.6-m s^{-1} wind was measured 2 m above the grass surface blowing left to right. Ignition was started by two field workers at the centre of the left-hand-side as shown in Fig. 1*a*. The workers then walked in opposite directions and took over 56 s to complete the line ignition. Fig. 1*b* shows the simulation from the current study at a time comparable with Fig. 1*a*.

Simulation domain

The simulation domain was 960 m long, 640 m wide and 100 m high. The inlet was prescribed as (1/7) power law model of the atmospheric boundary layer (ABL) (Morvan *et al.* 2013) with wind speed varied (3 to 10 m s^{-1}) 2 m above the ground, U_2. At 660 m from the inlet in the longitudinal direction, the burnable grass plot (104 $\times$ 108 m) was placed so that there was another ~200-m subdomain downstream of the plot before reaching an open outlet. On the lateral sides, ~270-m bordering subdomains were placed on either side of the burnable grass plot. Previous work showed that spread rates and fire behaviour were nearly identical if the subdomains upstream of, downstream of and bordering the burnable grass plot were increased beyond this arrangement. These subdomains had grid resolutions of 1 to 2 m in longitudinal (x) and lateral (y) directions and 0.25 to 1 m in the vertical (z) direction (finer resolution close to the burnable grass plot and coarser away from it). To avoid potential numerical instabilities, an aspect ratio not more than 2 for any grid cell was maintained. The subdomains containing burnable grass had a 0.25-m grid in all directions (for the grid-converged simulations) up to a height of 6 m above the grass surface. The simulations show that isosurfaces of heat release rate (HRR) (HRR per unit volume >80 kW m^{-3} was taken as a visual boundary to the visible flame) observed through FDS-WFDS's companion software *Smokeview* did not exceed 2 m height. That is, the visible flame was only ever ~2 m from the ground and well contained within the fine mesh. Above 6 m, grid cell sizes of 1 $\times$ 1 $\times$ 0.5 m were used.

Domain size, that is the non-burning grass area leading to, upstream and downstream of and bordering the burnable grass plot, may affect RoS and fire behaviour because of the influence of numerical boundary conditions on the flow. Domain height may also play an important role if the atmospheric boundary layer is not adequately resolved. In the present study, trial-and-error testing was adopted with fuel parameters presented in Table 1 to confirm that the domain size does not influence the RoS results. Table 2 presents three different domain set-ups and Fig. 2 shows the HRR and flame propagation results. The importance of these two parameters is discussed later. For both parameters, the results of 1320 $\times$ 760 $\times$ 120-m and 960 $\times$ 640 $\times$ 100-m cases are almost identical, though the HRR is a bit higher for the larger domain. This may be due to some asymmetry in the larger domain, which elongates the fire isochrones. However, 640 $\times$ 400 $\times$ 60-m (smaller) domain case results are completely different, proving that 960 $\times$ 640 $\times$ 100-m is adequate for this study.

Fuel model

In the simulations reported here, the Boundary Fuel (BF) model is adopted. The BF model is designed to simulate surface fuels such as grasslands (Mell *et al.* 2007).

The burnable material is considered to be a thin layer on the bottom boundary. The BF model uses a separate vertical computational grid for the fuel bed. This grid has a sufficiently

Table 1. Thermophysical, pyrolysis and combustion parameters for grass fire modelling

Input parameters	Values used	Source and reason
Heat of combustion	16400 kJ kg^{-1}	Bluestem grass (Overholt *et al.* 2014)
Soot yield	0.008 g g^{-1}	White pine (AbuBakar 2016)
Vegetation drag coefficient	0.125	Assuming vegetation elements are spherical (Morvan and Dupuy 2004)
Vegetation load	0.283 kg m^{-2}	Mell *et al.* 2007 – experimental
Vegetation height	0.21 m	Mell *et al.* 2007 – experimental
Vegetation moisture content	0.063	Mell *et al.* 2007 – experimental
Surface-to-volume ratio of vegetation	9770 m^{-1}	Mell *et al.* 2007 – experimental
Vegetation char fraction	0.17	Average of Mell *et al.* 2007 and bluestem grass (Overholt *et al.* 2014)
Vegetation element density	440 kg	White pine (AbuBakar 2016)
Vegetation bulk density: veg. load/veg. height	Determined (kg m^{-3})	
Ambient temperature	32°C	Mell *et al.* 2007 – experimental
Relative humidity	40%	Mell *et al.* 2007
Emissivity	0.99	Mell *et al.* 2007
Vegetation heat of pyrolysis (Δh_{pyr})	200 kJ kg^{-1}	White pine (AbuBakar 2016)
Maximum mass loss rate	0.15 (kg s^{-1} m^{-3})	Mell *et al.* 2007 – experimental; maximum amount of fuel allowed to be pyrolysed

Table 2. Parameters for domain sensitivity

Simulation name	Domain size	Distance of ignition line from inlet	Bordering subdomain (both sides)	Distance from plot end to outlet
Selected domain	960 m long × 640 m wide × 100 m height	660 m	~270 m	~200 m
Larger domain	1320 m long × 760 m wide × 120 m height	900 m	~330 m	~320 m
Smaller domain	640 m long × 440 m wide × 60 m height	440 m	~170 m	~100 m

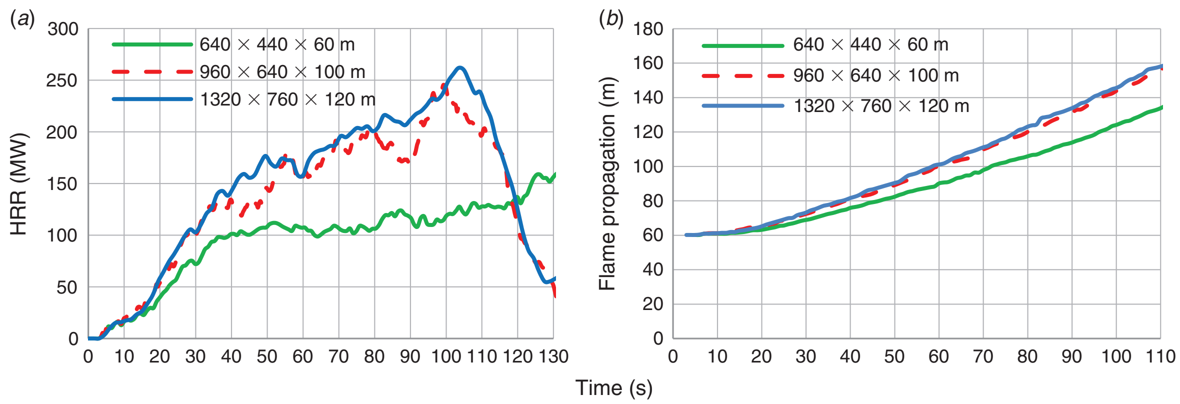

Fig. 2. Domain sensitivity results: (*a*) heat release rate (HRR); and (*b*) flame propagation.

high spatial resolution to capture the vertical radiant heat transfer. The horizontal grid is the same as the gas phase and the accuracy of convective heat transfer will be heavily influenced by the gas-phase grid resolution. The assumptions leading to the BF model are most consistent with large fires for which the majority of the heat release (and, therefore, radiant emission) occurs above the fuel bed (resulting in predominantly vertical radiant heat transfer in the thermally degrading fuel bed). Fuels such as tall grasses exert drag forces on the prevailing wind. The BF model accounts for the fuel drag by an aerodynamic drag force of the form:

$$F_{D,i} = -c_D \alpha u_i u_i, \tag{1}$$

where c_D and α are parameters estimated by considering each blade of grass as a cylinder, u is the mean velocity in the longitudinal direction and i represents each of the three coordinates.

The alternative model provided in WFDS is the Fuel Element (FE) model. In the FE model, the fuel is represented by individual particles located near and above the ground. Although this model is slightly more faithful to reality, it requires a prohibitively fine grid (i.e. too computationally demanding) to capture the physical processes in the fuel bed. In this model, the extinction length (δ_R) characterising the absorption of radiation by vegetation, which is the governing length scale in the vegetation fuel bed (Morvan 2011), needs to be resolved. δ_R can be obtained as 4/(packing ratio $\times$ surface-to-volume ratio), and packing ratio can be obtained from vegetation load, height and element density (Perez-Ramirez *et al.* 2017). Using the values presented in Table 1, the value of δ_R for the fuel bed used in the present study is 0.134 m. To resolve this fuel bed in the FE model, the grid size within the fuel bed needs to be lower than δ_R, and Mell *et al.* (2007) suggested grid size be one-third of δ_R, i.e. 0.045 m. This condition cannot be met using the FE model while also having a sufficiently large domain given currently available computational resources and numerical approaches. When the fuel bed cannot be appropriately resolved, the BF model is the alternative despite losing a part of the ability to calculate the physics of flow inside the fuel bed (Morvan 2011). As the vertical grid resolution is determined by δ_R constraints, the BF model is typically less computationally demanding than the FE owing to the coarser gas-phase grid (Mell *et al.* 2007). For more information on the precise formulation of each of these models, see Mell *et al.* (2007, 2009) and Perez-Ramirez *et al.* (2017).

Thermal degradation

In WFDS, there are two models for thermal degradation: a linear and an Arrhenius model. Both are based on empirical studies. Each degradation model can be used with each vegetation model. This leads to a total of four possible implementations to model a grassland fuel. We chose the BF model of vegetation with the linear model of fuel degradation. This choice was made to reduce the overall spatial resolution requirements, and therefore the computational time of the simulation. Briefly, the linear model assumes a two-stage endothermic thermal decomposition: water evaporation followed by solid fuel pyrolysis. The evaporation step is:

$$\dot{m}_{vap} = \frac{\dot{Q}_{net}}{\Delta h_{vap}} \text{ if } T_s = 373\,\text{K}, \tag{2}$$

where T_s is the vegetation surface temperature, $\dot{m}_{vap}$ is the evaporation rate, $\dot{Q}_{net}$ is the net energy (convection plus radiation) on the fuel surface and Δh_{vap} is the latent heat of evaporation. The temperature-dependent mass loss rate expression of Morvan and Dupuy (2004) (presented as Eqn 3) is used to model the solid fuel degradation and assumes that pyrolysis begins at T_0 and terminates at T_1:

$$\dot{m}_{pyr} = \frac{\dot{Q}_{net}}{\Delta h_{pyr}} \frac{T_s - T_0}{T_1 - T_0} \text{ if } T_0 \leq T_s \leq T_1, \tag{3}$$

where $\dot{m}_{pyr}$ is the pyrolysis rate and Δh_{pyr} is the heat of pyrolysis (also known as heat of reaction). In this study, in the absence of a measurement for this particular species, T_0 and T_1 are taken as 400 and 500 K respectively, in accordance with Morvan and Dupuy (2004). For other species, this range is estimated to have higher values, such as for lucerne hay, a cured herbaceous fuel (Wadhwani *et al.* 2017*b*). The solid fuel is represented as a series of layers that are consumed from the top down until the solid mass reaches a predetermined char fraction at which point the fuel is considered consumed. Char oxidation is not accounted for because significant char oxidation only occurs at material temperatures much greater than we achieve in these simulations. It is likely that with the 400–500-K range in the linear model, ignition and sustained burning occur at low adjacent gas-phase (air) temperatures. Because of this, coarser gas-phase grid resolutions may be sufficient but require the user to supply a bound on the maximum mass loss rate per unit volume (kg s^{-1} m^{-3}). In the Arrhenius model, drying, pyrolysis and char oxidation occur following separate Arrhenius equations, obtained from Porterie *et al.* (2005). The Arrhenius equations has the following form:

$$\dot{m} = m\beta \frac{dY}{dT} = mA\mathrm{e}^{\left[-\frac{E}{RT_S}\right]} \tag{4}$$

where β is the rate at which the material is heated, E is the activation energy of the reaction, m is the mass of the fuel, Y is the mass fraction of conversion to gaseous fuel and A is called the pre-exponential factor. R is the universal gas constant (8.31×10^{-3} kJ mol^{-1} K^{-1}). The material parameters may be obtained from the thermogravimetric analysis (TGA) of a small sample of the material. It can be seen that the Arrhenius model requires significantly more user-supplied parameters compared with the linear model. Furthermore, these parameters are difficult to measure accurately for wildland fuels and vary considerably with species (Wadhwani *et al.* 2017*a*). Therefore, we adopt the linear model of fuel degradation.

Conductive, convective and radiative heat transfer submodels used to calculate T_s for Eqns 3–4 are described in Perez-Ramirez *et al.* (2017).

Parameters used in the simulations

All the thermophysical, pyrolysis and combustion parameters are presented in Table 1. Parameters such as vegetation height and load are self-explanatory. The other parameters have been discussed above. The fuel parameter values are all selected to match the experiments of Cheney *et al.* (1993). Char fraction, heat of combustion, heat of pyrolysis and soot yield are selected to match recent measurements of cellulosic fuel.

A fire model can be sensitive to thermophysical, pyrolysis and combustion parameters that are inputs to the model. We did not perform a sensitivity study on any of these parameters (such as on the ones given in Table 1) here. We find that for the grass fires considered in this work, the RoS is well predicted using the BF and linear pyrolysis models. A sensitivity study may be required in the future when other fuel distributions and particular fuel species are considered.

Wind field development, grid convergence and validation results

Several numerical parameters: grid resolution, boundary layer development time and domain size, are considered for a systematic modelling approach. Open wind speed is the primary factor in determining fireline propagation. In all operational models, the wind is considered well developed over the fire ground. That is, that there are no significant changes in wind speed over the fire ground. In these simulations, we supply an inlet condition that is a power-law wind profile model. The flow will trip and become turbulent, leading to a developing boundary layer flow. Therefore, we need to examine the wind field over the fire ground to ensure that it does not change significantly in space and time. The sensitivity of the fire spread to a spatially developing boundary layer is not explored here and the question of how the simulated fire spread results change in a spatially varying wind field remains open. This problem may be the subject of a future study of numerical sensitivity.

Wind field development

In Mell *et al.* (2007), the boundary layer was driven by a 1/7th-power-law model, just as we apply here. However, in the FDS validation suite (McGrattan *et al.* 2017), the mean background wind velocity was incorporated by a nudging process. In the present study, we endeavour to obtain an appropriately mapped wind profile above the grassland within the fire simulation subdomain. The profile is expected to follow a logarithmic relation (Harman and Finnigan 2007):

$$\frac{u(z)}{u^*_{ABL}} = \frac{1}{k}\ln\left(\frac{z-d}{z_0}\right) \quad (5)$$

where z is the height above the surface, $u(z)$ is the velocity at z, u^*_{ABL} is the ABL friction velocity, κ is the von Karman constant (approximately 0.41) (Pope 2001), d is called the displacement length and z_o is the roughness length scale. z_o is variously suggested as 0.026 m (Su *et al.* 2001) and 0.05 m (Sutton 1953) for thick and thin grasses respectively. Because we model flow over a complicated grass surface, an equivalent z_o may be determined from the simulations. The equivalent roughness length will depend on the leaf area density, essentially the ratio of surface area-to-volume of the grass, as well as the grass height and other parameters of the flow (Harman and Finnigan 2007). Varying the grass height and fuel load will cause variation in the equivalent z_o. The simulated flow over the grassland yields a measurement, by a fitting procedure (Bou-Zeid *et al.* 2004), of the equivalent z_o specific to the fuel parameters used in the simulation. It is not the aim of this manuscript to characterise the behaviour of equivalent z_o for grasslands. Here, d is the displacement height due to the presence of the grass layer. u^*_{ABL} can be estimated from the $u(H)$, where H is any height close to the top domain boundary, as:

$$u^*_{ABL} = \frac{\kappa u(H)}{\ln(\frac{H}{z_o}) - 1} \quad (6)$$

Prior to the actual simulation of fire line spread, precursor simulations were carried out to simulate the ABL above the grassland within the simulation domain. Precursor simulations were conducted without grass burning until a steady-state ABL developed over the length of the domain. It appears that 160 s is required for wind of $U_2 = 6$ m s^{-1} to travel from the inlet to the outlet approximately (domain length/U_2), and that timescale can be termed as the domain travel time (DTT). In Fig. 3, longitudinal velocity profiles at various downwind locations along the centreline are plotted at various points in time. These figures show how the boundary layer develops. Minor perturbations in the flow cause turbulence to develop. The turbulence will alter the mean flow profile both in time and space. After ~1.66 DTT, the ABL reach a quasi-steady state with only minor variations in the velocity profile between 1.66 and 3.75 DTT. The most significant variations in the flow occur downstream of the burnable plot area as the flow adjusts to the outlet boundary. We allow the ABL to evolve for 5 DTT to ensure that the fire simulations are conducted under conditions of fully developed flow. The results of the precursor ABL simulation are stored in data files and used as the initial velocity fields for the actual grass fire simulations.

To check the robustness of the ABL simulation, non-dimensional velocity profiles, $\frac{u(z)}{u^*_{ABL}}$ are plotted against $\frac{1}{k}\ln(\frac{z}{z_0})$, from four simulations where U_2 velocities at inlet are 3, 6, 7.5 and 10 m s^{-1} in Fig. 4. These profiles are taken 100 m upstream of the ignition line locations at the centre of the domain. All four profiles reasonably collapse on each other and a clear logarithmic layer is visible. The log-law, i.e. Eqn 5, is found to be parallel to, and above, the simulation result. This shifted log-law is due to the effect of the grass canopy on the flow. The quantification of the displacement height has not been explored further in this study.

Grid convergence

The choice of the size of the grid (cell) in a mesh is one of the first and most important decisions one must make while developing an input file script for a simulation. The choice of grid size can affect the results, and therefore a grid convergence study needs to be conducted to ensure the results are not significantly sensitive to the choice of grid size, thus to obtain grid-converged results. However, convergence may require an inordinate cost of computing resources. Previously, grid-converged results were elusive owing to the high computational costs. Here, we will demonstrate that grid-converged results of grass fire simulations are possible. Grid convergence means that the numerical results are as accurate as possible. However, grid convergence does not improve acknowledged modelling errors, such as modelling the drag of the grass as a distributed volume drag term.

In building fires, HRR is the primary variable (Moinuddin and Thomas 2009; Moinuddin *et al.* 2011). The HRR is essentially related to Byram's fire intensity (Byram 1959) multiplied by the length of the fire. Empirical models attempt to predict the RoS of fires. For that reason, we consider RoS as the primary variable for a grid convergence study. RoS is the most important parameter in characterising a wildland fire and other variables such as temperature and heat flux usually follow the same trend as the RoS. For grid convergence, the same simulation (unchanged boundary conditions) needs to be conducted with at least three different grid sizes and the RoS results compared. If RoS values are found to be approximately the same with finer grid sizes, one can be confident that the results are independent of the numerical grid.

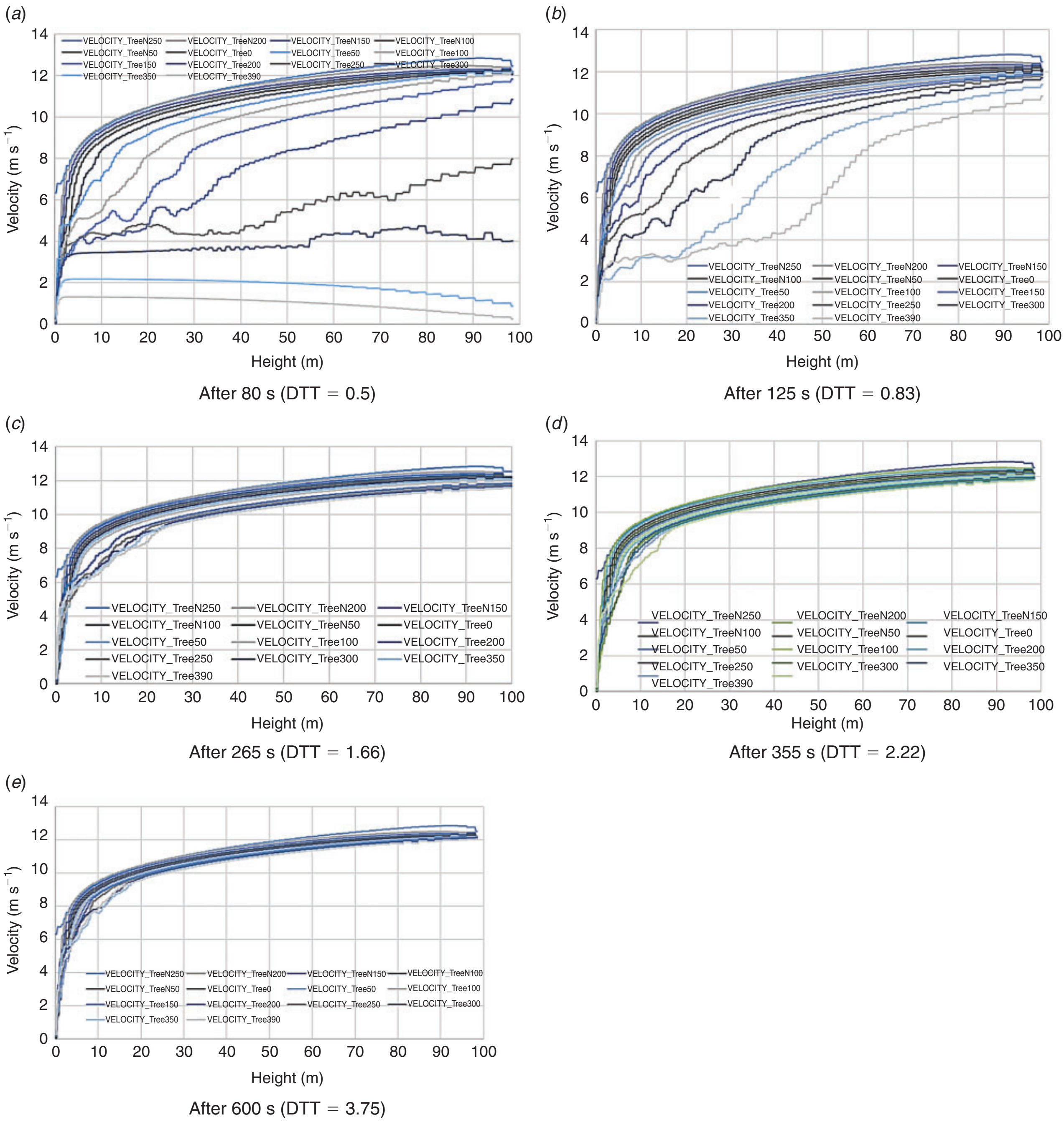

Fig. 3. Velocity profiles at various instances of time (DTT = domain travel time; VELOCITY_TreeNxxx and VELOCITY_Treexxx represent anemometer tree xxx m before and after the ignition line respectively).

To determine the required grid size, a smaller domain was used containing the burnable grass plot with proportional bordering no-burning subdomains. Three successively finer grid spacings of 0.5, 0.25 and 0.167 m in all three spatial directions in the subdomains containing burnable grass were used for the simulations. The flame front positions as a function of time results are compared in Fig. 5. It can be seen that RoS (slope of the plotted flame front propagation distance vs time) results are almost identical for the 0.25- and 0.167-m grids. Hence, the results are declared grid-converged at a grid spacing of 0.25 m. Two stretched grids were also used (named 0.25-sp5, representing the grid cell height adjacent to the surface, $\delta z_{nearwall} = 0.125$ m expanding to 0.5 m at the top of the domain, and 0.25-sp25, representing $\delta z_{nearwall} = 0.0625$ m similarly expanding to 1 m). It can be seen that 0.25-sp5 and 0.25-sp25 do not provide a systematic pattern in relation to non-stretched cases, nor do the RoS results on these grids converge to a grid-independent value.

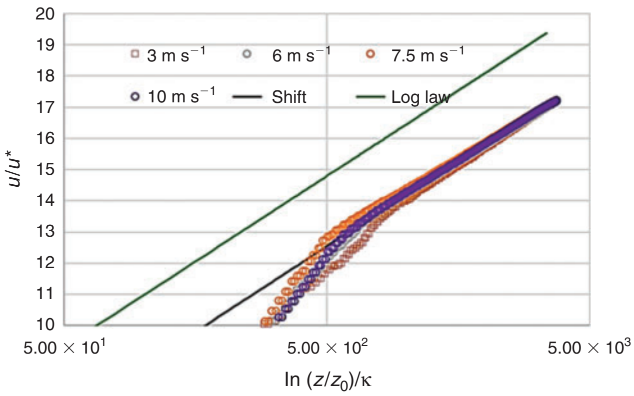

Fig. 4. Non-dimensional semilogarithmic velocity profiles at various inlet velocities.

Validation case

Following Mell *et al.* (2007), we repeat the case that Mell et al. label C064 case and compare it with experimental results for validation; however, we use significantly a higher resolution to ensure grid-converged simulations. For the model validation, the appropriate wind condition needs to be established. Cheney *et al.* (1993) recorded wind speeds at the north west (NW) and south-west (SW) corners of the plot 2 m above the ground. When the inlet was prescribed as a power-law (1/7) wind model with 6- and 6.5-m s^{-1} wind speed at 2 m, near-experimental wind speed was obtained. In Fig. 6, the time history of wind speeds (averaged over 5 s) during the burn from the simulation and physical observation is presented. Fig. 6*a* shows that with the 6-m s^{-1} inlet condition, the wind speed is slightly (~6%) under-predicted. However, in Fig. 6*b*, simulated wind flow is

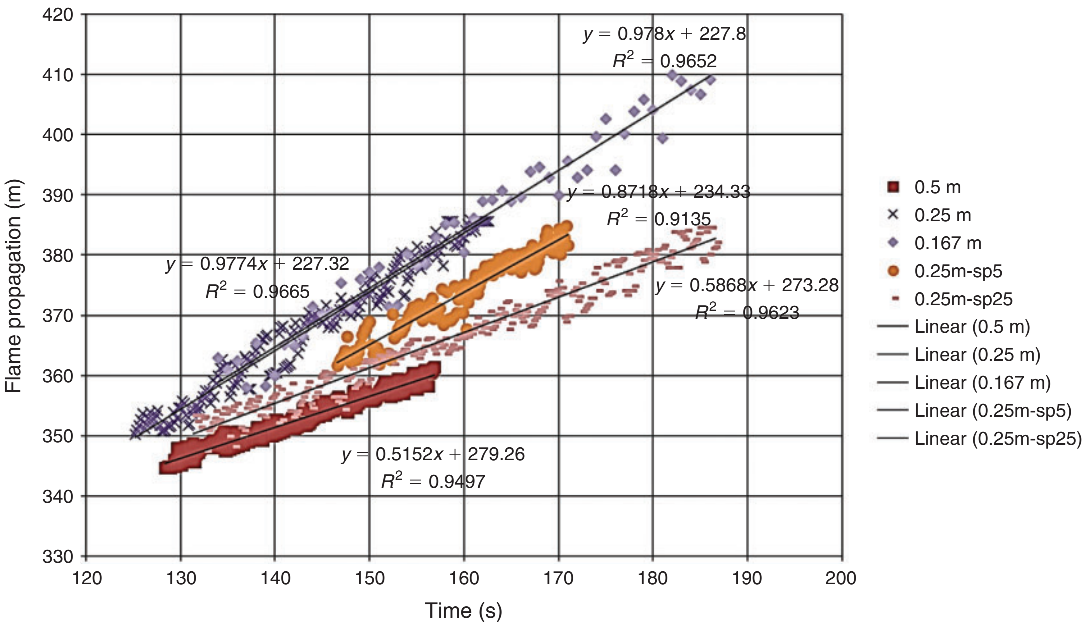

Fig. 5. Flame propagation distance as functions of time.

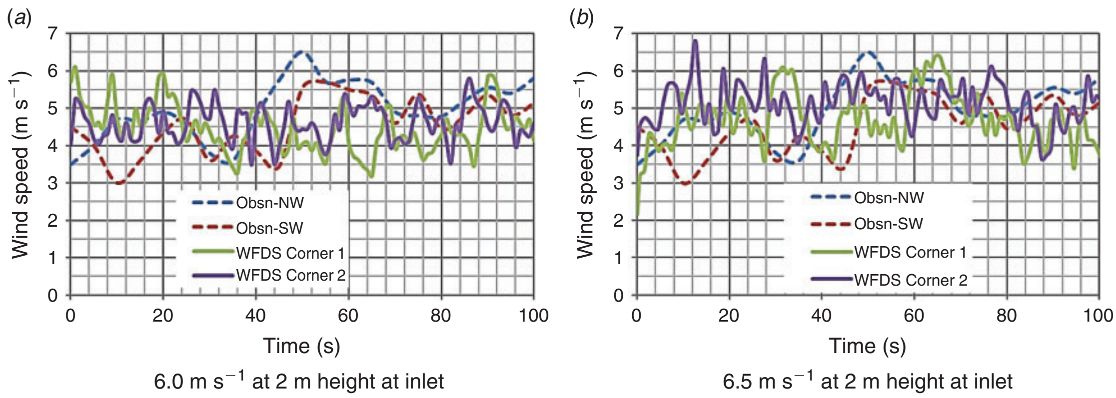

Fig. 6. Measured and simulated wind speeds at the upwind corners of the burn plot. Two different inflow conditions are shown: (*a*) 6 m s^{-1} at 2-m height; (*b*) 6.5 m s^{-1} at 2-m height. Obsn represents physical measurement.

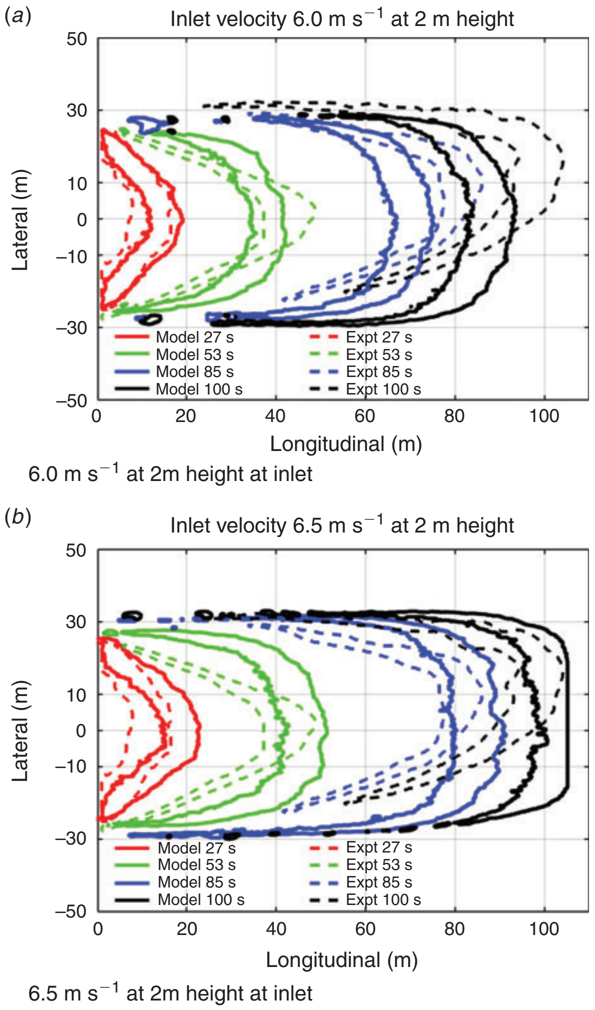

Fig. 7. Model validation: fire propagation.

marginally (~2%) overpredicted. Wind gusts are observed in both the experimental and simulated data.

Morvan (2014) simulated the propagation of a grass fire using a 2-D numerical model. The cases considered were fire spread driven by constant wind speeds of 1-, 2- and 3-m s^{-1} and fires driven by wind speeds that varied sinusoidally between 1 and 3 m s^{-1} with periods of 1 and 2 s. This is a significantly faster variation than was observed experimentally here but is comparable with the frequency of variation in our simulations. Morvan (2014) found that there was no significant deviation from the steady 2-m s^{-1} RoS in the cases where the wind speed varied; effectively, the fire was not able to respond to the fast variations in wind speed. However, in the experimental fires, the period of the gust is significantly greater (see for example Fig. 6*a*) and the fire may respond to the gust behaviour. Hence, understanding the sensitivity of the fire spread to the driving wind speed is important.

In Fig. 7, the fire perimeter from the experimental study and two simulations (with $U_2 = 6$ and 6.5 m s^{-1}) are compared at different times. The fire spread occurs from left to right. The fire perimeters are plotted 27, 53, 85 and 100 s after the start of ignition. It can be seen that fireline progression is reasonably well predicted overall. The simulated fire line contours appear to lag behind the experimental contours for the 6-m s^{-1} driving wind by ~10 m (or 10%) at the end of the simulation, but for the 6.5-m s^{-1} driving wind, the simulated contours lead the experimental contours by ~5 m at the end of the simulation. We attribute this discrepancy largely to how the fire contours are determined. Experimentally, the fire contours are determined by the location of the visible flame above some colour threshold. For the simulations, the fire contour is defined as the region on the boundary where the temperature of the vegetation is above 400 K (the pyrolysis temperature). Although the two methods of identifying the front should be comparable, small differences can be expected. Towards the back of the flame, the ground temperature will be large but the flame will be almost extinguished because no fuel remains. At the front edge of the fire, the visible flame may be longer than the pyrolysis region, particularly if the flame is leaning downwind.

A more obvious discrepancy between the simulated and observed contours is on the flanks of the fire perimeter: the simulated fire front is much flatter than the experimental fire front and the apparent centre of the fire moves away from the centreline of the domain. We hypothesise that these effects in the experimental fire front are due to variation in the lateral wind speed. No lateral wind speed is considered in the simulations and it was not measured in the experiments. The effect of lateral wind speed on the shape of the fire front requires further study, but is not considered here.

Comparing the experimental contours with the simulated contours is a complicated task. The main aim is to provide some estimate of the size of the error in the simulation of a real-world fire. There are many potential sources of this error. In the simulated and experimental results presented in Fig. 7, the head of the experimental fire does not continue to propagate in a straight line. This deviation is probably due to a change in wind direction during the experimental burn. There is no such deviation in the simulation results because the wind direction is kept constant in the simulation. Further complicating the comparison between the experimental and simulated fire contours is the development of thin flanks on the simulated fire compared with the experimental fire. To quantify the differences between the simulated and experimental fire contours, we examine separate measures of error for the difference in fire centre location and the difference between the fire flanks.

A cartoon illustrating the measures of difference that we computed is shown in Fig. 8.

First, we define the centre of the fire isochrone in the following manner: a line is drawn from the maximum longitudinal point, called p_1, on the isochrone (effectively the very tip of the fire) to the geometric centroid of the isochrone contour. The geometric centroid of the fire contour is

$$\overrightarrow{x_c} = \frac{\int \vec{x} I(\vec{x}) d\vec{x}}{\int I(\vec{x}) d\vec{x}} \quad (7)$$

where the $\overrightarrow{x_c}$ is the (vector) representing the centroid location and $I(x)$ is an indicator function that takes the value 0 if the coordinates $\vec{x}$ are outside the contour and value 1 if the coordinates $\vec{x}$ are inside the fire contour.

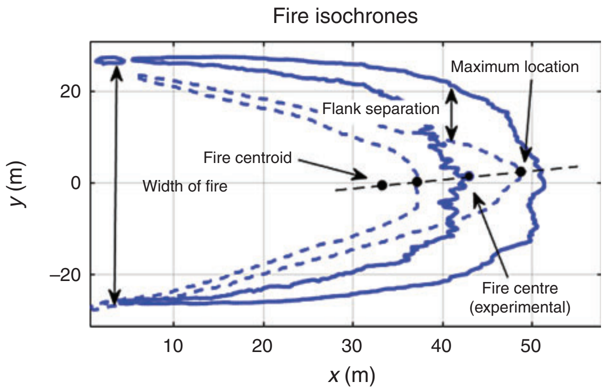

Fig. 8. Cartoon showing how the measures of error are constructed. The experimental contour is shown as a blue dashed line and the simulation is the solid blue line.

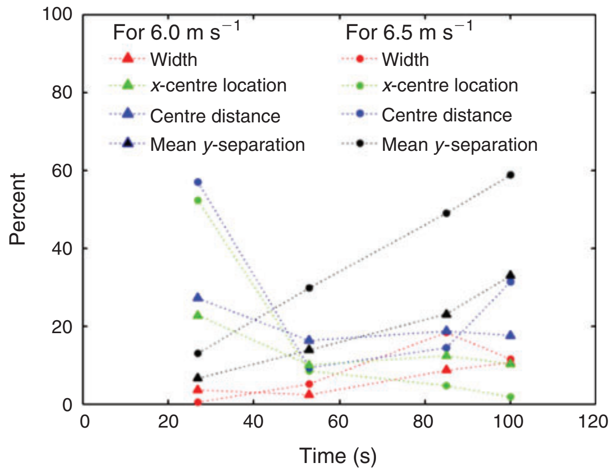

Fig. 9. The measures comparing the experimental fires (triangles) with the simulated fires (circles).

The point where the line intersects with the 'inner' part of the contour is then identified and called p_0. The fire centre is defined as the midpoint $p_c = (p_1 - p_0)/2 + p_0$. The fire centre is a coordinate in the xy plane. The fire centres for the experimental and simulated contours are compared in two ways: the Euclidean distance between them $((x_1 - x_0)^2 + (y_1 - y_0)^2)^{1/2}$, where the centre of the experimental fire $(x_0, y_0)$is at simulated fire is at (x_1, y_1) and the absolute difference in the x direction is computed and the percentage differences relative to the location of the experimental fire centre are plotted in Fig. 9 for both $U_2 = 6$ and $U_2 = 6.5$ m s^{-1}.

To compare the fire width, we computed the maximum width of the fire and compared the differences in the maximum width between the simulation and experiments. The percentage differences relative to the width of the experimental fire, for both $U_2 = 6$ and $U_2 = 6.5$ m s^{-1}, are shown in Fig. 9. Finally, the maximum distance between the fire flanks was measured and the percentage differences relative to the width of the experimental fire were plotted for both $U_2 = 6$ and $U_2 = 6.5$ ms^{-1}, shown in Fig. 9. Typically, all measures of error are below 30%, indicating that there is decent agreement between the simulation and experiment. The error plots do, however, show that minor differences in wind speed and direction can significantly affect the simulated results. In the experimental fire, based on the motion of the isochrones, there was likely an increase in wind speed and a change in direction ~30 to 60 s after the fire was lit. The gust leads to an acceleration and a slight change in direction of the fire. The change of direction appears as a very large error in the flank distance measurement. Similarly, starting with $U_2 = 6.5$ m s^{-1} leads to large errors in fire centre location, suggesting that $U_2 = 6.5$ m s^{-1} is faster than the experimental wind speed, at least initially.

The good agreement in terms of RoS and reasonable agreement in terms of fire front shape demonstrate that WFDS with the particular fuel model used here can be used, with some confidence of physical fidelity, for a parametric study of grass fires.

Comparison of simulations with experimental results and empirical models – effect of wind speed

So far, only a single validation comparison has been made between a numerical simulation and a particular experiment. It is instructive to consider how a set of simulation results compares with a set of observed fires. Although in principle a set of direct comparisons is possible, appropriately matching all parameters is not practical. In any case, many discrepancies attributable to known differences between the experimental and simulated conditions will be observed. Nonetheless, such a comparison between simulated and experimental results will demonstrate if the simulation delivers realistic results. Similarly, it is interesting to compare operational models, derived from experiment, with the simulated results. In this case, the empirical models can be applied with exactly the same parameters as considered in the simulation. This comparison highlights differences in trends between the models and also helps to identify biases and limitations in all of the models. Finally, such a comparison demonstrates the feasibility of constructing statistical models from physics-based simulations.

Empirical models typically take inputs such as open wind speed, often 10 m above the ground (U_{10}), some measure of fuel dryness and some atmospheric data. Recently, there has been a discussion in the scientific community regarding the appropriate parameters to use in empirical models (Sharples 2017). Essentially, Sharples argues real grass fires and wildland fires have inherently complicated and chaotic dynamics. The inclusion of independent variables in the empirical models to account for fine-scale variation may be an unwise modelling choice, and wherever possible the simplest models that adequately explain the data should be preferred. Physics-based simulations are inherently detailed, with multiple parameters that require estimation. The sensitivity of physics-based models to all parameters has not been completely assessed. Given the number of parameters in a physics-based model, a comprehensive investigation of all possible sensitivities is computationally prohibitive. However, from physics-based modelling where parameters can be varied systematically, it is, therefore, possible to develop a statistical model from a fit to RoS from some independent variable. Here, we chose wind speed as the independent variable because it is regarded as the dominant parameter in fire spread (Cheney *et al.* 1998).

We compare our physics-based model with the McArthur grass fire models, and the CSIRO grass fire model. Noble *et al.* (1980) presented a set of equations for the McArthur fire spread models. The Mk III (Mark 3) version of the model is

$$\mathrm{RoS} = 0.26\ \exp(-23.6 + 5.01\log(C) + 0.0281T - 0.226H^{1/2} + 0.633U_{10}^{1/2})\ldots\ldots \quad (8)$$

in which U_{10} is as described above, T is the air temperature (°C), H is the relative humidity (as a fraction) and C is the curing index. Curing index is a measure of the fraction (%) of dried grass in the grassland. The higher the green component, the lower the C, and consequently its ignitability is lower.

In the Mk V (Mark 5) version of the grassland fire danger meter, the *RoS* is modelled as a function of fire danger index (F):

$$\mathrm{RoS} = 0.13F \quad (9)$$

in which F is presented as a function of fuel weight, W (tonnes ha^{-1}), average wind velocity, U_{10} (km h^{-1}) and fuel moisture content, MC (%):

$$F = 3.35W \times \exp(-0.0897MC + 0.0403U_{10}) \quad (10a)$$

when $MC < 18.8\%$

$$F = 0.299W \times \exp(-1.686MC + 0.0403U_{10}) \times (30 - MC) \quad (10b)$$

when $18.8\% < MC < 30\%$

MC is a function of T, H and C:

$$MC = \frac{97.7 + 4.06H}{T + 6} - 0.00854H + \frac{3000}{c} - 30 \quad (11)$$

Cheney *et al.* (1998) proposed an alternative model (known as the CSIRO model):

$$RoS = \begin{cases} (0.054 + 0.209U_{10})\phi M\ \phi C, U_{10} \le 5\,\mathrm{km\,h^{-1}} \\ (1.1 + 0.715(U_{10} - 5)^{0.844})\phi M\ \phi C, U_{10} > 5\,km\,\mathrm{h}^{-1} \end{cases}\ldots\ldots \quad (12)$$

where φM is the fuel moisture coefficient and φC is the curing coefficient. The curing coefficient is

$$\phi C = 1.12/[1 + 59.2\exp\{-0.124(C - 50)\}] \quad (13)$$

In turn, φM is given by:

$$\phi M = \begin{cases} \exp(-0.108MC), MC < 12\% \\ 0.684 - 0.0342MC, MC \ge 12\%,\ U_{10} < 10\,km\,\mathrm{h}^{-1} \\ 0.547 - 0.0228MC, MC \ge 12\%, U_{10} \ge 10\,\mathrm{km\,h^{-1}} \end{cases} \quad (14)$$

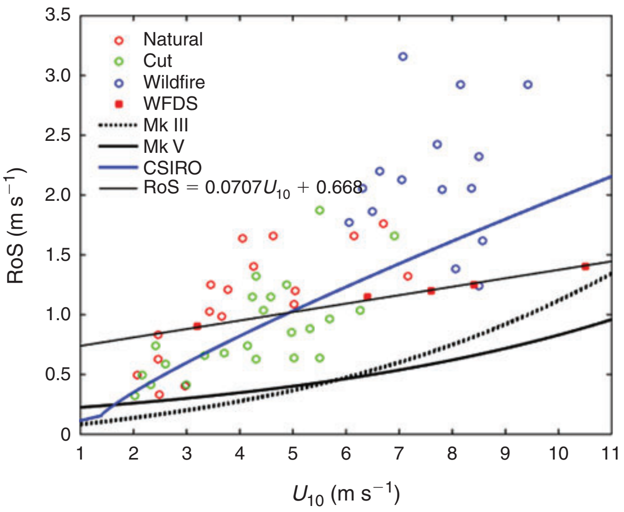

Fig. 10. Rate of spread vs 10-m open wind speed for the simulated grasslands, compared with operational models with experimental results obtained by Cheney *et al.* (1993) placed in the background.

It should be noted that the CSIRO model is constructed to have a discontinuity in predicted RoS at a windspeed of 5 km h^{-1}. The CSIRO model depends linearly on wind speed below the critical wind speed and is a power law (with exponent 0.844) above the critical wind speed. Cheney *et al.* (1998) made this modelling choice because the experimental fires at wind speeds below 5 km h^{-1} tended to not propagate in a quasi-steady state and a linear fit to the data was found to be reasonable in this region.

In the present study, we conducted several simulations of grass fires where wind speed varies, in order to compare the findings with Eqns 8, 9 and 12 as well as physical or experimental observations. The parameters are the same as provided in Table 1. The only variation is U_2 at the inlet, which is varied between 3 and 10 m s^{-1} (3, 6, 6.5, 7.5 and 10 m s^{-1}). The RoS was found to be strongly linear with wind speed.

In Fig. 10, the simulated RoS of the head fire as a function of U_{10} (U_{10} values are obtained from the data presented in Fig. 4) is compared with operational models while the experimental observations obtained by Cheney *et al.* (1993) are placed in the background. It is our intention to compare simulated RoS with experimental observations in order to judge the faithfulness to reality of the physics-based models, and to compare physics-based modelling of RoS with predictions of RoS from operational models with the same parameters.

The experimental grass fires were conducted under a range of fuel and ambient weather conditions. The grass height also varies: natural grass refers to undisturbed or ungrazed pasture land, cut grass refers to mowed (and likely removed) or grazed pasture lands including crop stubble, and wildland fire is from a set of 20 major grassland fires in south-eastern Australian from 1965 to 1990. The CSIRO model is derived from this experimental dataset whereas the two McArthur models (Mk III and Mk V) were derived from a dataset of lower wind speed range. The CSIRO model is therefore expected to be a good fit for this dataset.

The WFDS simulations predict significantly higher RoS at 3-m s^{-1} wind speed than the CSIRO and McArthur (Mk III and Mk V) models; however, the simulated RoS is realistic when compared with the experimental fires of Cheney *et al.* (1993). At the higher limit of wind speed, above U_{10} of 6 m s^{-1}, the WFDS simulation predicts a significantly lower RoS than the CSIRO model, but higher than both McArthur models. The discrepancy at higher velocities may be due to the effect of fireline size, which was not investigated here. The experimental observations are RoS from wildland fires rather than experimental fires, where the fireline size is not controlled.

Rate of spread as a function of grass height

The dependence of RoS on grass height is a matter of debate. Anecdotal evidence from fire agencies suggests that if the grass height is higher, the RoS of the headfire is larger. Recent experiments conducted in Victoria, Australia, (Cruz *et al.* 2016) suggest that RoS does not depend on the grass height. Observations from gamba grass fires in the Northern Territory of Australia reported by fire agencies suggest that there may be some dependence of RoS on the grass height (S. Heemstra, pers. comm. 2016). It is important to note several points about these observations. First, the fuel types and conditions that lead to these anecdotal observations are quite varied. Second, the invasive species gamba often grows to a much greater height than the native grasslands of south-eastern Australia, and therefore height is much more likely to influence the fire behaviour.

In order to investigate the dependence of RoS on grass height, we conduct simulations of grass fires representative of native grasslands, varying grass height between 100 and 600 mm. The results of the simulations presented here are only representative of the conditions used in the simulations and may not hold for a different set of parameters. Nonetheless, these results shed light on dependence on grass height and it is useful for fire agencies to have a correlation between RoS of the fire and grass height to assist in strategic decision-making, even if the correlation can only be developed for a single fuel type at present.

A set of simulations was carried out with seven different grass heights: 0.1, 0.14, 0.175, 0.21, 0.315, 0.475 and 0.6 m at inlet U_2 of 6.0 m s^{-1}. Here, the vegetation load is varied proportionally to the grass height to maintain a constant bulk density. That is, the grass is not considered to be mowed and left on the ground.

The HRR vs time curves are presented for all seven cases in Fig. 11*a*. The 0.1-m case shows that the fire self-extinguishes early. Four cases (0.6, 0.475, 0.315 and 0.21 m) have the same trend in HRR. Two cases, 0.14 and 0.175 m, effectively saturate at a significantly lower HRR. This observation is consistent with two modes of propagation. This follows the observation of Apte *et al.* (1991) for industrial fires in polymer sheets. Apte *et al.* (1991) found that as the fire became more intense, the buoyant forces from the fire overcame the shearing forces of the background wind and the flame became more vertical as the fire propagated in the so-called plume mode. In this case, the boundary layer mode has lower HRR and plume mode has higher HRR and correspondingly greater buoyant forces. In the first mode, the flame is bent over and confined to a boundary

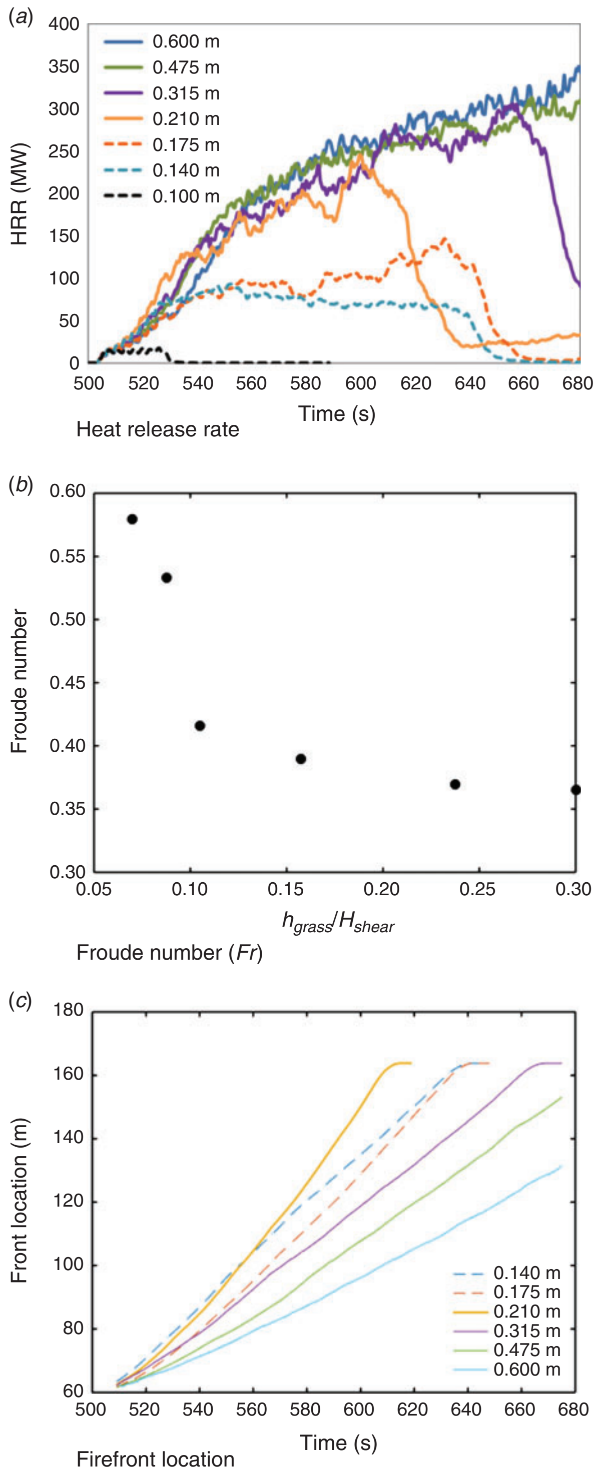

Fig. 11. Effect of vegetation height. (*a*) Heat release rate (HRR) as a function of time; and (*b*) Froude number (*Fr*) as a function of grass height; and (*c*) location of fire fronts as a function of time. The 0.14- and 0.175-m cases are in boundary layer mode of propagation; the 0.6-, 0.475-, 0.315- and 0.21-m cases in plume mode of propagation. In the plume mode, increasing grass height in these simulations leads to a decrease in the rate of spread.

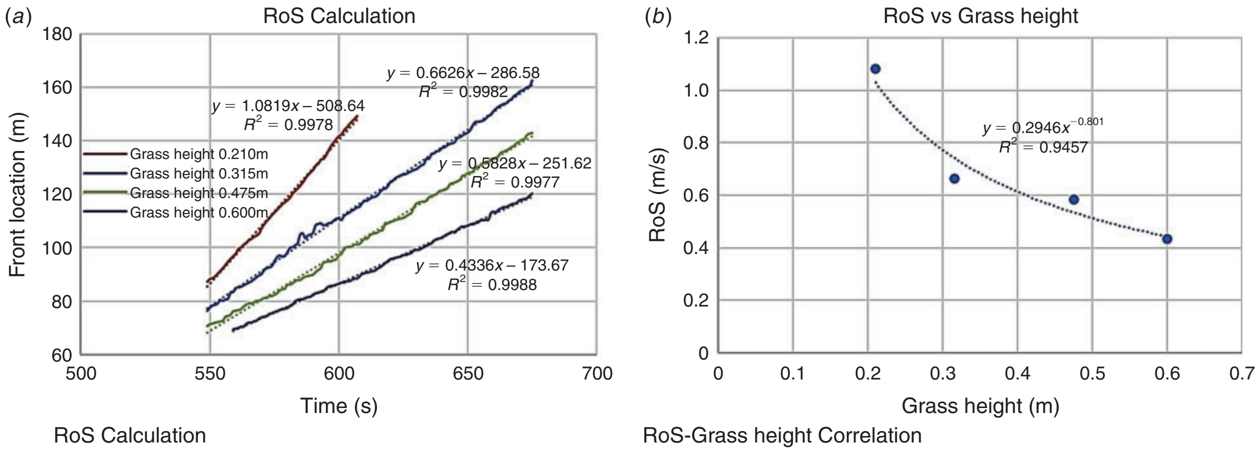

Fig. 12. Development of rate of spread (RoS)–grass height correlation. (*a*) RoS calculation when RoS reached steady state; and (*b*) least-squares method analysis of RoS against grass height.

layer flow and in the second mode, the flame is more vertical and plume-like. Similar effects have been noted for grass fires and proposed as an explanation of the surge–stall mechanism of fire spread (Dold 2011).

During the establishment period of the fire, all of the cases are in boundary layer mode and the fire front is highly influenced by the wind flow within the boundary layer. Once the fire reaches a certain HRR threshold, large enough for buoyancy-induced flow to have a controlling influence on fire behaviour, the fire switches to the plume mode of propagation. The 0.14-m case did not reach that threshold – so it remained in boundary layer mode. The 0.175-m case remained in boundary layer mode for most of the duration and then possibly switched to the plume mode at the end of the simulation.

The Froude number (Fr), which is the ratio of inertial forces to buoyancy forces, is calculated with Eqn 15:

$$Fr = \frac{U_{10}}{\{gHRR/(\rho C_p T_S)\}^{1/3}} \tag{15}$$

where g is the acceleration of gravity, ρ is the density of the fuel and C_p is the specific heat capacity of the fuel. The HRR is taken over the quasi-steady region (after approximately 550 to 620 s) and an average maximum solid temperature over the same time is chosen. In Fig. 11*b*, Fr is plotted against the non-dimensional grass height (normalised by $H_{shear} = 2$ m, which is considered as the midpoint of the flame height). There is a sharp decrease in Fr as the grass height increases. This again suggests two modes of fire behaviour (Apte *et al.* 1991) and the threshold appears to be approximately $Fr = 0.5$. These simulations show that as the grass height increases, the larger amount of fuel available results in more fuel pyrolysis and larger fire sizes, eventually leading to the fire front overcoming the boundary layer effect.

In Fig. 11*c*, the locations of the headfire as a function of time are presented (the slope of each curve represents RoS). Leaving aside the 0.14-m (boundary layer mode) and the 0.175-m (mostly boundary layer mode) fuel height cases, a clear trend in RoS emerges for the plume mode propagation (0.21-m case onwards). In the plume mode (the 0.6-, 0.475-, 0.315- and 0.21-m height cases), the RoS decreases as the grass height increases. Physically, these differences may be understood by considering the heat transfer from the flame to the unburnt vegetation. In the boundary layer mode, the flame is inclined towards the ground and the virgin fuel ahead of the fire front; this leads to the unburnt vegetation receiving high net convective and radiative heat flux in the boundary layer mode. As a result, virgin fuel ahead of the fire front quickly undergoes pyrolysis and the RoS is large, whereas in the plume mode, the net heat transfer to the virgin fuel decreases as the flame becomes more vertical owing to buoyancy-induced flow towards the fire front. The lower heat transfer to the unburnt vegetation leads to a lower RoS.

To develop a RoS–grass height correlation, a least-squares method analysis is conducted in Fig. 12. In Fig. 12*a*, RoS for each grass height in plume mode is calculated when steady-state conditions were reached. In each case, the R^2 value is ~0.998, reflecting that they are truly in steady state. Fig. 12*b* shows a power-law relation between RoS and grass height with an R^2 value of 0.95. A linear fit to the same data results in $R^2 = 0.83$. The fit shows that for constant wind speed and fuel conditions, the RoS depends non-linearly on the grass height. Ultimately, a much larger dataset would be required to establish a comprehensive model of RoS in terms of grass height by taking into account variation in wind speed or different fuel moisture conditions, etc.

Conclusions

Fires in grasslands are prevalent in Australia and other countries, and are fairly simple to model computationally owing to the uniform fuel and flat simple terrain. For a systematic modelling approach, we considered several numerical parameters: grid resolution, boundary layer development time and domain size for WFDS compatible with FDSv6. RoS results were converged on a 250-mm (cubed) grid. The ABL was allowed to evolve for 5 DTTs to ensure that the fire simulations were conducted under conditions of fully developed flow.

We then used a CSIRO grassland experiment as the validation case and the simulation results were found to be valid. It should be noted that only a single validation comparison is presented between a numerical simulation and a particular experiment. Although in principle a set of direct comparisons between simulation results and observed fire is possible, we cannot have access to all the 3D distribution of every fundamental variable to appropriately match. Thus, validation of physics-based models is a very complex task and indirect validation, which shows that the simulation delivers realistic results, can build confidence among model developers, researchers and potential users such as fire behaviour analysts. Consequently, validation must be always considered as an ongoing process. Once good agreement was obtained with grid-converged results, a study was conducted where the background wind speed and the grass height were varied independently. When wind speed is varied, the WFDS model predicts a faster fire spread rate than both the Mk III and Mk V (McArthur) models, but typically a slower RoS than the CSIRO model for wind speeds greater than U_{10} of 6 m s^{-1}. In addition, the RoS was found to be linear with wind speed in the parameter range considered.

Seven simulations were conducted where the bulk density of the fuel was kept constant as height varied. In these simulations, it was observed that as the grass height increases, the fire front changes from boundary layer mode to plume mode. Once the fire fronts are in plume mode, higher grass height results in bigger fires, but a slower RoS. A least-squares analysis shows that within the grass height range considered in the plume mode, a power-law relationship exists between the RoS and grass height.

To construct statistical models from physics-based simulations, parametric studies can be expanded to other topographical, fuel and weather parameters. Some of the concerns expressed by fire behaviour analysts (S. Heemstra, pers. comm. 2016) are related to density, volume ratio, moisture and heterogeneity (patchiness) of fuel, sloped terrain, temperature and humidity of air, and soil moisture, etc. Such parametric study can lead to the improvement of the current operational implementation models. The improved models will be helpful for fire authorities in developing their strategies in the management of firefighting and evacuation logistics in order to plan the risk from fire spread so that risks and losses associated with wildland fire can be reduced.

Conflicts of interest

The authors declare no conflicts of interest.

Acknowledgements

This research was funded by the Bushfire and Natural Hazards Cooperative Research Centre (CRC) and computational resources were provided by the University of Melbourne Research Platforms.

References

AbuBakar AS (2016) Characterization of fire properties for coupled pyrolysis and combustion simulation and their optimised use. PhD thesis, Victoria University, Melbourne, Australia. Available at http://vuir.vu.edu.au/31007/ [Verified 12 October 2018]

Apte V, Bilger R, Green A, Quintiere J (1991) Wind-aided turbulent flame spread and burning over large-scale horizontal PMMA surfaces. *Combustion and Flame* **85**, 169–184. doi:10.1016/0010-2180(91)90185-E

Bou-Zeid E, Meneveau C, Parlange MB (2004) Large-eddy simulation of neutral atmospheric boundary layer flow over heterogeneous surfaces: blending height and effective surface roughness. *Water Resources Research* **40**, W02505. doi:10.1029/2003WR002475

Bureau of Meteorology (2009) Bushfires in Victoria, 7–8 February 2009. Available from: http://www.bom.gov.au/vic/sevwx/fire/20090207/20090207_bushfire.shtml [Verified 12 April 2018].

Bureau of Transport Economics (2001) Economic costs of natural disasters in Australia. Bureau of Transport Economics Report 103, January 2001, pp. iii–170. (Canberra, Australia)

Byram GM (1959) Forest fire behavior. Forest Fire: Control and Use. (Ed. KP Davis) (McGraw-Hill: New York).

Cheney N, Gould J, Catchpole WR (1993) The influence of fuel, weather and fire shape variables on fire-spread in grasslands. *International Journal of Wildland Fire* **3**, 31–44. doi:10.1071/WF9930031

Cheney N, Gould J, Catchpole WR (1998) Prediction of fire spread in grasslands. *International Journal of Wildland Fire* **8**, 1–13. doi:10.1071/WF9980001

Chong D, Tolhurst K, Duff T (2012) PHOENIX RapidFire 4.0 convection and ember dispersal model. (Bushfire CRC: Melbourne, Vic., Australia). Available at http://www.bushfirecrc.com/sites/default/files/phoenix_4_convection_and_spotting.pdf [Verified 12 April 2018].

Cruz MG, Andrew S, Susan K, Richard H, David N (2016) The effect of grass curing and fuel structure on fire behaviour: final report. CSIRO Report no. EP166414. (Canberra, Australia) Available at https://publications.csiro.au/rpr/download?pid=csiro:EP166414&dsid=DS1 [Verified 12 April 2018]

Dold J (2011) Fire spread near the attached and separated flow transition, including surge and stall behaviour. In 'Proceedings of the 19th International Congress on Modelling and Simulation', 12–16 December 2011, Perth. pp. 200–206.

Harman IN, Finnigan JJ (2007) A simple unified theory for flow in the canopy and roughness sublayer. *Boundary-Layer Meteorology* **123**, 339–363. doi:10.1007/S10546-006-9145-6

Linn RR, Canfield JM, Cunningham P, Edminster C, Dupuy JL, Pimont F (2012) Using periodic line fires to gain a new perspective on multidimensional aspects of forward fire spread. *Agricultural and Forest Meteorology* **157**, 60–76. doi:10.1016/J.AGRFORMET.2012.01.014

McArthur AG (1967) 'Fire behaviour in eucalypt forests.' (Forestry and Timber Bureau: Canberra)

McDermott RJ (2014) A velocity divergence constraint for large-eddy simulation of low-Mach flows. *Journal of Computational Physics* **274**, 413–431. doi:10.1016/J.JCP.2014.06.019

McGrattan KB, Hostikka S, McDermott RJ, Weinschenk C, Forney GP (2013) 'Fire dynamics simulator, user's guide', 6th edn. NIST Special Publication 1019. (U.S. Department of Commerce: Maryland)

McGrattan KB, Hostikka S, McDermott RJ, Floyd J, Weinschenk C, Overholt K (2015) 'Fire Dynamics Simulator – technical reference guide volume 1: Mathematical model. FDS Version 6.2.0 edn.' (U.S. Department of Commerce: Maryland)

McGrattan KB, Hostikka S, McDermott RJ, Floyd J, Vanella M, Weinschenk CG, Overholt K (2017) 'Fire Dynamics Simulator, technical reference guide volume 3: Validation, 6th edn.' NIST Special Publication 1018–3. (U.S. Department of Commerce: Maryland)

Mell W, Jenkins MA, Gould J, Cheney P (2007) A physics-based approach to modelling grassland fires. *International Journal of Wildland Fire* **16**, 1–22. doi:10.1071/WF06002

Mell W, Maranghides A, McDermott R, Manzello SL (2009) Numerical simulation and experiments of burning Douglas fir trees. *Combustion and Flame* **156**, 2023–2041. doi:10.1016/J.COMBUSTFLAME.2009.06.015

Miller C, Hilton J, Sullivan A, Prakash M (2015) SPARK – A bushfire spread prediction tool. In 'International Symposium on Environmental

Software Systems', 25–27 March 2015, Melbourne. pp. 262–271. (Springer: Cham, Switzerland)

Moinuddin K, Thomas IR (2009) An experimental study of fire development in deep enclosures and a new HRR–time–position model for a deep enclosure based on ventilation factor. *Fire and Materials* **33**, 157–185. doi:10.1002/FAM.986

Moinuddin K, Al-Menhali JS, Prasannan K, Thomas IR (2011) Rise in structural steel temperatures during ISO9705 room fires. *Fire Safety Journal* **46**, 480–496. doi:10.1016/J.FIRESAF.2011.08.001

Morvan D (2011) Physical phenomena and length scales governing the behaviour of wildfires: a case for physical modelling. *Fire Technology* **47**, 437–460. doi:10.1007/S10694-010-0160-2

Morvan D (2014) Wind effects, unsteady behaviors, and regimes of propagation of surface fires in open field. *Combustion Science and Technology* **186**, 869–888. doi:10.1080/00102202.2014.885961

Morvan D, Dupuy J (2001) Modeling of fire spread through a forest fuel bed using a multiphase formulation. *Combustion and Flame* **127**, 1981–1994. doi:10.1016/S0010-2180(01)00302-9

Morvan D, Dupuy J (2004) Modeling the propagation of a wildfire through a Mediterranean shrub using a multiphase formulation. *Combustion and Flame* **138**, 199–210. doi:10.1016/J.COMBUSTFLAME.2004.05.001

Morvan D, Méradji S, Accary G (2009) Physical modelling of fire spread in grasslands *Fire Safety Journal* **44**, 50–61. doi:10.1016/J.FIRESAF.2008.03.004

Morvan D, Méradji S, Mell W (2013) Interaction between head fire and backfire in grasslands. *Fire Safety Journal* **58**, 195–203. doi:10.1016/J.FIRESAF.2013.01.027

Noble I, Gill A, Bary G (1980) McArthur's fire-danger meters expressed as equations. *Australian Journal of Ecology* **5**, 201–203. doi:10.1111/J.1442-9993.1980.TB01243.X

Overholt K, Cabrera J, Kurzawski A, Koopersmith M, Ezekoye OA (2014) Characterization of fuel properties and fire spread rates for little bluestem grass. *Fire Technology* **2014**, 9–38.

Parliament of New South Wales (2009) Victorian Bushfires – condolence motion, March 2009. http://www.parliament.nsw.gov.au/prod/parlment/hansart.nsf/v3key/la20090313005 [Verified 12 December 2010]

Perez-Ramirez Y, Mell WE, Santoni PA, Tramoni JB, Bosseur F (2017) Examination of WFDS in modeling spreading fires in a furniture calorimeter. *Fire Technology* **53**, 1795–1832. doi:10.1007/S10694-017-0657-Z

Pope SB (2001) 'Turbulent flows.' (IOP Publishing: Cambridge)

Porterie B, Consalvi JL, Kaiss A, Loraud JC (2005) Predicting wildland fire behavior and emissions using a fine-scale physical model. *Numerical Heat Transfer, Part A: Applications* **47**, 571–591. doi:10.1080/10407780590891362

Sharples JJ (2017) A unified approach to fire spread modelling. In 'Proceedings of Bushfire and Natural Hazards CRC & AFAC annual conference 2017', 4–6 September 2017, Sydney, Australia. pp. 201–205. (Bushfire and Natural Hazard CRC, Sydney)

Su Z, Schmugge T, Kustas WP, Massman WJ (2001) An evaluation of two models for estimation of the roughness height for heat transfer between the land surface and the atmosphere. *Journal of Applied Meteorology* **40**, 1933–1951. doi:10.1175/1520-0450(2001)040<1933:AEOTMF>2.0.CO;2

Sutton OG (1953) 'Micrometeorology: a study of physical processes in the lowest layers of the Earth's atmosphere.' (McGraw-Hill: New York, NY, USA)

Wadhwani R, Sutherland D, Moinuddin KAM, Joseph P (2017*a*) Kinetics of pyrolysis of litter materials from pine and eucalyptus forests. *Journal of Thermal Analysis and Calorimetry* **130**, 2035–2046. doi:10.1007/S10973-017-6512-0

Wadhwani R, Sutherland D, Moinuddin K (2017*b*) Suitable pyrolysis model for physics-based bushfire simulation. In 'Proceedings of 11th Asia–Pacific Conference on Combustion', 10–14 December 2017, Sydney, Australia. pp. 582–585. (The Combustion Institute: Australian and New Zealand section, Sydney)